Assimilation of Clear- and Cloudy-Sky Upper-Tropospheric Humidity Estimates Using *GOES-8* and *GOES-9* Data

LOUIS GARAND AND JACQUES HALLÉ

Atmospheric Environment Service of Canada, Dorval, Quebec, Canada

(Manuscript received 15 July 1996, in final form 8 January 1997)

ABSTRACT

A strong linearity exists between the 6.7-μm clear-sky outgoing brightness temperature (BT) and dewpoint depression (DPD) at upper-tropospheric levels. A similar relationship, using the logarithm of relative humidity instead of DPD, was developed by Soden and Bretherton. Here, however, the humidity at specific levels is derived as opposed to the humidity integrated over upper-tropospheric levels. Linear relationships are obtained between a 6-h model forecast of DPD and calculated BTs at different viewing angles. The data are further stratified in terms of 400-mb temperature as an indicator of airmass type. Applying these relationships using observed 6.7-μm BTs and a 6-h forecast of 400-mb temperature yields vertically correlated estimates of DPD between 200 and 500 mb, with DPD typically decreasing with height, and corresponding rms error estimates in the range 3–6 K. The retrieval technique is applied to *GOES-8* and *GOES-9* data, which cover about 40% of the globe. In cloudy regions, proxy humidity estimates based on cloud classification are used. These clear- and cloudy-sky DPD estimates are assimilated every 6 h in a global forecast model, taking into consideration the horizontal correlation of the error. The system is supplemented by quality-control procedures.

In parallel runs at the Canadian Meteorological Centre, the analyses and forecasts with satellite data (SAT) were found significantly improved with respect to those without satellite data (NOSAT). The system was therefore implemented. The superiority of the SAT forecasts in terms of 6.7-μm BT, 2-K versus 4-K rms at initial time, gradually decreases to the level of the NOSAT forecasts in 48 h. A slight improvement on geopotential, DPD, and temperature is observed in 48-h forecasts with respect to radiosondes over North America. The new upper-tropospheric DPD retrieval technique is robust and could easily be applied to other geostationary or polar-orbiting platforms providing 6.7-μm imagery.

1. Introduction

In recent years, the meteorological community has recognized the importance of better monitoring atmospheric water vapor, including that of the upper troposphere, both for climatic and numerical weather prediction (NWP) applications (see Soden and Bretherton 1994; McMillin et al. 1995; Bates et al. 1996; Blakwell and McGuirk 1996; Salathé et al. 1995; McNally et al. 1995; Macpherson et al. 1996). For NWP, satellite information on humidity is extracted mostly from three infrared channels in the 6.5–8.2-μm region available from polar-orbiting satellites. Similar channels are available on *GOES-8* and *GOES-9* (Geostationary Operational Environment Satellite) providing data over chosen sectors (not full disks). Retrievals of low-level water vapor (mostly below 600 mb) can also be derived from Special Sensor Microwave/Imager (SSM/I) channels over oceans (see, e.g., Deblonde et al. 1995; Phalippou 1996).

The scope of this paper is to present a new retrieval technique providing clear-sky upper-tropospheric humidity profiles (UTH, 600 mb and above) from the 6.7-μm imaging channel of *GOES-8* (75°W) and *GOES-9* (135°W) and to evaluate the impact of these data in NWP. The retrievals are introduced in the so-called Humsat (humidity from satellite) system, which provides proxy humidity estimates based on cloud classification (following Garand 1993, hereafter GA93). The assimilation system to be evaluated therefore includes both clear air and cloudy estimates. Emphasis is put on the new UTH clear-sky retrieval technique as other components of the Humsat system were previously described in GA93. This article, however, reports for the first time on the impact of Humsat data in NWP.

Interesting aspects of the GOES water vapor imaging channel include the high temporal (full disks every 3 h) and horizontal (8 km) resolution along with simultaneous visible (1 km) and infrared window channels (4 km) data. Schmetz and Turpeinen (1988) were the first to develop a UTH product from the 6.7-μm channel in the form of a mean 300–600-mb relative humidity. The expected link between upper-tropospheric humidity

Corresponding author address: Dr. Louis Garand, Atmospheric Environment Service, 2121 Trans-Canada Highway, Dorval, PQ H9P 1J3, Canada.
E-mail: louis.garand@ec.gc.ca

and dynamics was later demonstrated (Schmetz et al. 1995) from UTH observations. Soden and Bretherton (1993, 1996) showed that the logarithm of UTH is directly proportional to the water vapor brightness temperature (BT) and used that property to infer climatic variations in UTH. The linearity was shown to hold over almost the entire range of humidity; more precisely, departure from linearity becomes apparent only at very low humidities, 2% or less (Schmetz et al. 1995). Similarly here, we used the fact that dewpoint depression (DPD is the air temperature minus wet bulb temperature) is linearly related with BT, which could have been guessed from the fact that the logarithm of RH and DPD are highly correlated (correlation exceeding 99%). The choice of DPD was originally motivated (see GA93) by the fact that operational NWP analyses at the Canadian Meteorological Centre use DPD as a humidity variable. In the present application, however, a major difference is that BT is related to the humidity at *specific levels*, rather than to a mean UTH. As a consequence, the data can be assimilated easily in the same manner as radiosondes (assimilation of an integrated quantity is somewhat more complicated). It also turns out that the UTH is not uniform, climatologically, over the range sensed by the 6.7-μm radiance: it tends to decrease. This behavior and the error assignment by level are made explicit in the chosen approach. In addition, for climatic applications, the UTH is more clearly defined from values at specific levels on a global basis. Indeed, the 6.7-μm radiance is sensitive to higher levels in the Tropics (200–400 mb) than in polar regions (400–600 mb), which implies that the UTH retrieved from methods mentioned above must be interpreted in terms of these different pressure levels.

The linear relations at the base of the technique are stratified in terms of satellite viewing angle and 400-mb temperature, the latter being the only ancillary quantity (it is obtained from a 6-h forecast). The impact on forecasts is evaluated in parallel assimilation cycles differing solely by the use or nonuse of the satellite humidity estimates. Other important aspects of the system are estimates in cloudy regions, error correlation, and quality control. The method is presented in section 2. Section 3 describes the horizontal and vertical correlation of the errors, and section 4 describes the quality-control procedures. Section 5 presents the impact on NWP analyses and forecasts. Section 6 summarizes the article.

2. Retrieval method

a. General aspects

As originally designed, the Humsat cloud analysis system uses the infrared 11-μm channel and in daytime the visible channel to classify clouds in eight nighttime and ten daytime classes based on cloud height, albedo, and fraction at the scale of $1^\circ \times 1^\circ$. An additional class defines cumulonimbus (and a wet profile) whenever the cloud top is lower than 150 mb. In addition, the 6.7-μm water vapor channel is used to derive the humidity at levels 300–500 mb. The system was implemented at the Canadian Meteorological Centre (CMC) in June 1993 as applied to *GOES-7* data. A revised system was implemented in August 1995 that included quality-control procedures (Deblonde et al. 1995); the consideration of the correlation of errors (Garand 1994), an additional level at 925 mb interpolated (in specific humidity using the first-guess temperature profile) between the 1000- and 850-mb estimates, and an additional class corresponding to low-level broken stratocumulus; that system ran every 6 h until early January 1996 when *GOES-7* measurements stopped.

As mentioned in the introduction, this paper describes the new utilization of the water vapor channel as applied to *GOES-8* and *GOES-9* and the impact of Humsat data in assimilation cycles. While the original system used DPD versus BT fits based on collocated radiosondes with observed BT, the new system uses fits based on forecast DPD profiles and corresponding BTs calculated using a radiative transfer model (RTM). Provided the RTM is accurate (shown further), the advantages of the new approach are essentially that (i) relationships from everywhere on the globe and at all viewing angles can be derived; and (ii) known problems with upper-level humidity measurements from radiosondes are avoided, such as the lack of response at cold temperatures, the difference in instrument characteristics used in different countries, and the inability to provide DPD measurements above 250 or 300 mb. Furthermore, experience has shown that fits based on observed data tend to lack dynamic range (due to limitations mentioned above), while fits based on the physics of radiative transfer are superior in their ability to relate extremes of BT to extremes in DPD. The use of synthetic data, while possibly not ideal, appears to be the best way to get an ensemble covering possible atmospheric realizations on a global scale.

The following comments expand on the motivation for this work in an NWP context. The CMC, like several other NWP centers, is moving toward the direct assimilation of radiances through variational methods using about 20 (to start with) collocated sounding channels. Certainly, this methodology could be applied to the 6.7-μm imaging channel. However, the Humsat system provides over full geostationary disks independent information from that of sounding channels both in clear and cloudy areas every 6 h. The current operational strategy is thus to use the Humsat system with geostationary imaging channels in all sky conditions and to move toward the direct assimilation of clear sky radiances available from sounding channels onboard geostationary and polar-orbiting satellites.

b. Radiative transfer model

Assuming no scattering and a ground emissivity of unity, the basic radiative transfer equation to compute clear-sky upward infrared radiances is

TABLE 1. DPD rms error and DPD–TB correlation coefficient for nadir and 70° retrievals as a function of pressure level (mb) and air mass.

Level		150	200	250	300	350	400	500	570	620
(a) DPD rms error (K)										
T1	0°	3.0	4.0	4.0	3.7	4.1	4.5	6.6	7.4	8.0
	70°	3.0	3.5	4.0	3.9	4.5	5.4	7.3	7.9	8.4
T2	0°	3.0	3.7	3.8	4.5	3.6	3.8	6.0	7.5	8.1
	70°	3.0	3.2	3.1	3.9	3.5	4.2	7.0	8.2	8.7
T3	0°	3.8	3.8	3.6	3.6	3.9	3.5	3.9	4.6	5.2
	70°	3.5	3.3	3.0	3.1	3.4	3.2	4.3	5.1	5.6
T4	0°	5.1	4.7	3.7	4.0	5.0	4.2	4.0	3.8	4.0
	70°	5.1	4.4	3.4	3.6	4.5	3.9	3.9	4.1	4.2
(b) Correlation coefficient										
T1	0°	0.71	0.82	0.88	0.90	0.89	0.86	0.71	0.60	0.50
	70°	0.72	0.74	0.92	0.92	0.86	0.80	0.63	0.52	0.43
T2	0°	0.62	0.71	0.81	0.79	0.86	0.87	0.75	0.63	0.53
	70°	0.70	0.80	0.87	0.85	0.87	0.84	0.63	0.51	0.42
T3	0°	0.49	0.55	0.70	0.74	0.72	0.80	0.81	0.72	0.61
	70°	0.59	0.68	0.80	0.81	0.78	0.84	0.76	0.64	0.50
T4	0°	0.40	0.33	0.46	0.56	0.49	0.65	0.74	0.74	0.67
	70°	0.45	0.46	0.58	0.65	0.59	0.71	0.75	0.67	0.58

$$I_0 = B(p_s)t(p_s, p_0) + \int B(p')\frac{\partial t(p_0, p')}{\partial p}\,dp, \quad (1)$$

where B designates the Planck function, p_s the surface pressure, and t the atmospheric transmittivity; subscript 0 designates the top of the atmosphere, and p' in the integral varies from p_s to p_0. The brightness temperature is obtained from I_0 by inverting the Planck function, assuming an effective wavelength for the satellite band under study. The transmittivity from each level to the top of the atmosphere was computed using the classical approach of the Goody random model and the assumption of a Lorentz line shape (Liou 1980; Garand 1983; Rodgers and Walshaw 1966). Spectroscopic parameters at 10-cm^{-1} resolution from the HITRAN 1986 database (Rothman et al. 1986) were used.

For application to *GOES-8*, the spectroscopic parameters were averaged (Rogers and Walshaw 1966, appendix A) over the spectral range 1420–1540 cm^{-1}, the limits being chosen as the closest point where the normalized response function reaches the value 0.5. Following the notation in the above-mentioned publications (i.e., Table 1 in Garand 1983), the *GOES-8* imaging channel 3 spectroscopic parameters used are $k/\delta = 75.010$ m^2 kg^{-1} and $\pi a_0/\delta = 0.20911$, and parameters for temperature effects are $a = 1.5058 \times 10^{-3}$ K^{-1}, $b = -6.7754 \times 10^{-6}$ K^{-2}, $a' = 2.3505 \times 10^{-3}$ K^{-1}, and $b' = -6.7557 \times 10^{-6}$ K^{-2}. We used an effective wavelength of 6.744 μm found by a detailed spectral weighting of the Plank function at several temperatures times the *GOES-8* response function. *GOES-9* simulations were done with the same code because radiative transfer calculations indicated negligible differences in BT between the two sensors (these simulations are defined in section 2e). Only water vapor was considered as an active absorber.

The RTM as used here bypasses the detailed frequency integration. Errors, hopefully small, caused by a combination of imperfect measurements and an imperfect forward model are left to a final bias adjustment, assuming then that the bias is uniform over the range of observed BTs. Equation (1) was integrated at higher spectral resolution, using six bands. It was verified that most of the error translates into a bias constant over the entire range of BTs. The increased absorption by the water vapor continuum is another effect not considered here; Stephens et al. (1996) showed that including this absorption would reduce the BTs by about 2 K although the exact magnitude is still an object of debate. Finally, errors of a few tenths of a degree in the calibration of the observations are possible. Section 2e discusses how an overall bias correction was applied and presents an independent validation of the forward model from line-by-line calculations made available in the later stages of this research.

c. DPD versus BT relationships

The 6.7-μm brightness temperature is not affected by the surface term in (1) because of the very low transmittivity across the entire atmosphere, even in polar regions. Brightness temperature depends essentially on three inputs: the temperature profile, the humidity profile, and the viewing angle, the latter being known precisely. From clear-sky atmospheric profiles provided by a short-term forecast, BT was calculated at four viewing angles: 0°, 39°, 56°, and 70°, which represents linear increments of 0.22 in cosine of viewing angle. Since, in addition, it is known that BT has a peak response [usually inferred from the maximum of $\partial t/\partial p$ in Eq. (1)] from levels 300 to 500 mb, the data were stratified in four airmass types defined in terms of 400-mb temperature: T1: $T_{400} > 250$ K; T2: 240 K $< T_{400} <$ 250 K;

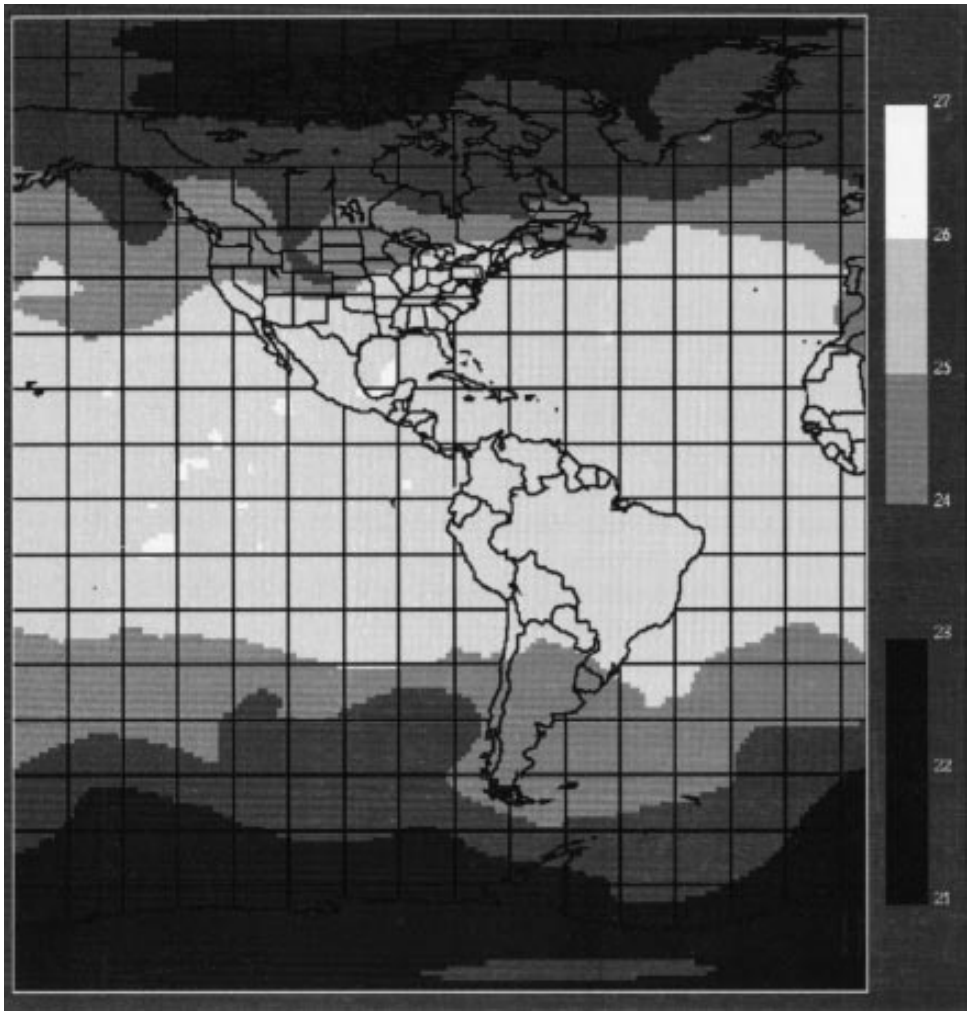

FIG. 1. The 400-mb temperature (K) of 6-h forecast valid at 1200 UTC 5 October 1995. Temperatures above 250 K define air mass T1; T2 has values between 240 and 250 K, T3 between 230 and 240 K, and T4 below 230 K (scale on the right: 24 means 240 K).

T3: 230 K $< T_{400} <$ 240 K; and T4: $T_{400} <$ 230 K. Figure 1 shows T_{400} for about half of the global domain used in fits. Loosely, T1 represents the Tropics and subtropics, T2 the midlatitudes, T3 sub-Arctic profiles, and T4 Arctic air masses. Clearly, this division makes more sense than one that would be based simply on latitude bands as there is asymmetry between hemispheres and intrusions of cold/warm air masses in latitudes that are on average warmer/colder. Here T_{400} is the only ancillary information necessary in the proposed retrieval scheme (other information is, however, used in quality-control procedures described in section 4 and in the determination of the cloud cover described in GA93). In practice, T_{400} is available to good precision (about 2.5-K rms) globally from a 6-h forecast. A total of 16 fits (four angles and four air masses) were obtained; the final estimate is a 2D interpolation between pairs of fits in terms of logarithm of cosine of viewing angle (found more appropriate than the cosine) and 400-mb temperature. The variance of the error is interpolated in the same manner.

Recently Soden and Bretherton (1996, hereafter SB96) improved their original formulation in order to consider the influence of the air mass. Their equation is

$$a + b\mathrm{BT} = \log_e[\mathrm{RH}\ \sec(\theta)\ p_0], \qquad (2)$$

where a and b are linear regression coefficients, and θ is the satellite viewing angle. The air mass parameter p_0 is defined as the UTH pressure where the temperature is 240 K (near 300 mb in the Tropics and 500 mb in polar regions) divided by 300 mb. We verified that this approach is equivalent to ours. Indeed, a map of p_0 has nearly identical patterns to those seen in Fig. 1 with T1 corresponding to $p_0 <$ 325 mb, T2 with 325 mb $< p_0 <$ 400 mb, T3 with 400 mb $< p_0 <$ 500 mb, and T4 with $p_0 >$ 500 mb. A major advantage of Eq. (2), however, is that it is universal (keeping in mind that in SB96 RH is the average integrated UTH with level RH layer

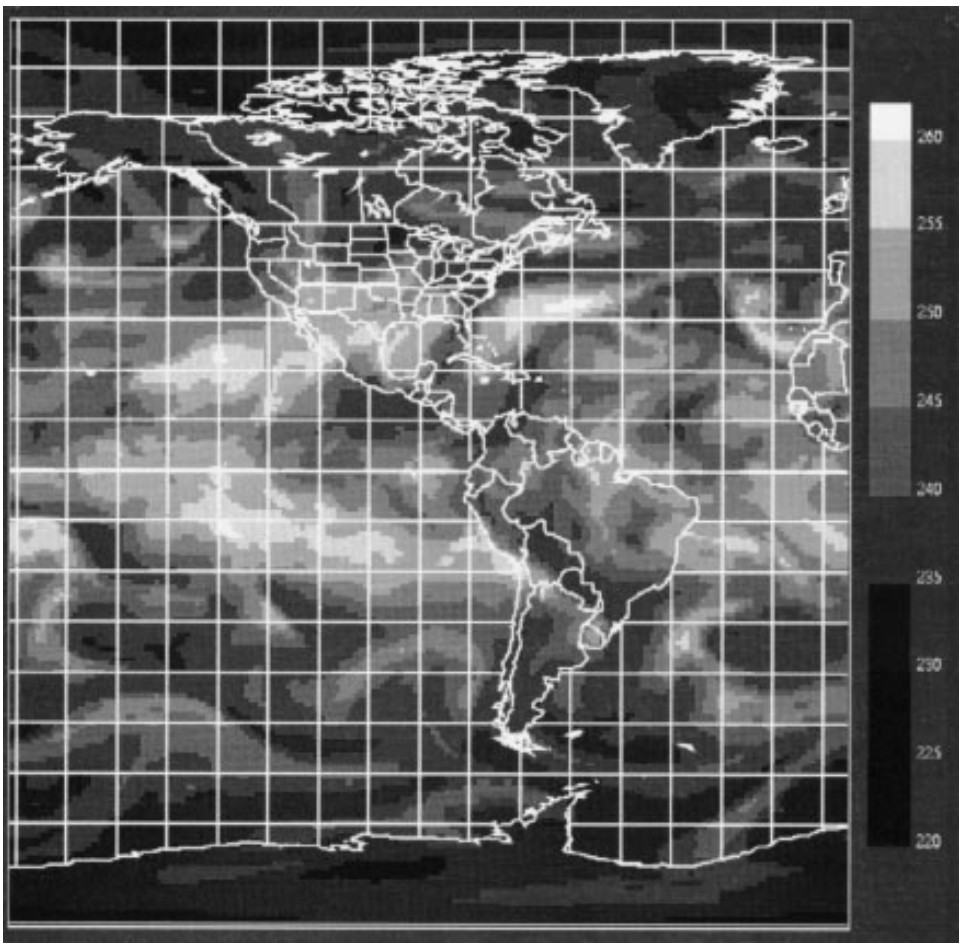

FIG. 2. (a) Calculated clear-air brightness temperature at nadir for the same case as in Fig. 1; (b) corresponding 400-mb DPD.

values weighted as a function of temperature; in the actual application to specific levels no such weighting would enter into play). We found that when (2) is applied, for a fixed viewing angle, at specific levels to each of the four individual air masses, DPD or RH rms errors very close to those from our approach are obtained. However, when a single universal fit is applied to individual air masses, results are degraded by a few tenths of a degree rms in DPD and DPD biases of the order of 1 K occur (dry bias in the Tropics, wet bias in the Arctic). Similarly, the explicit dependency on viewing angle leads to biases of the order of 0.5 K in DPD. For this reason, we kept our specific fits in viewing angle and air mass. Between latitudes 60°N and 60°S (excluding most of T3 and T4 profiles) considered in the SB96 study, airmass biases noted above are much smaller if the fit is based on data between these latitudes.

A single model realization, a 6-h global forecast valid at 1200 UTC 5 October 1995, was used as training dataset to derive the fits. This comprises 400 × 200 points, a dataset thought to be sufficient to properly represent the variability of atmospheric profiles. Coldest 400-mb temperatures in that case are 218 K; T_{400} below 215 K are rare even in polar night areas in January. The model horizontal resolution is similar (1° × 1°) to that of the Humsat parameter extraction system, which computes the average 6.7-μm radiance (then inverted to BT) within 1° squares to eventually be used in fits. Brightness temperature was computed assuming no clouds, and therefore the fits are valid for clear-sky conditions. It was judged preferable to use a short-term forecast rather than an analysis because current operational analyses stop at 300 mb (extrapolation above that level; a forecast will presumably organize high-level moisture in a more realistic fashion, in particular in zones of wind convergence/divergence) and DPDs are limited to 30-K DPD, which is too low of a threshold (values reaching 40 K are not uncommon, as discussed further). Figure 2a shows the calculated BT at nadir (again over half the domain) and Fig. 2b the corresponding 400-mb DPD. The strong correlation between the two fields is evident. Differences between nadir and 70° BTs can

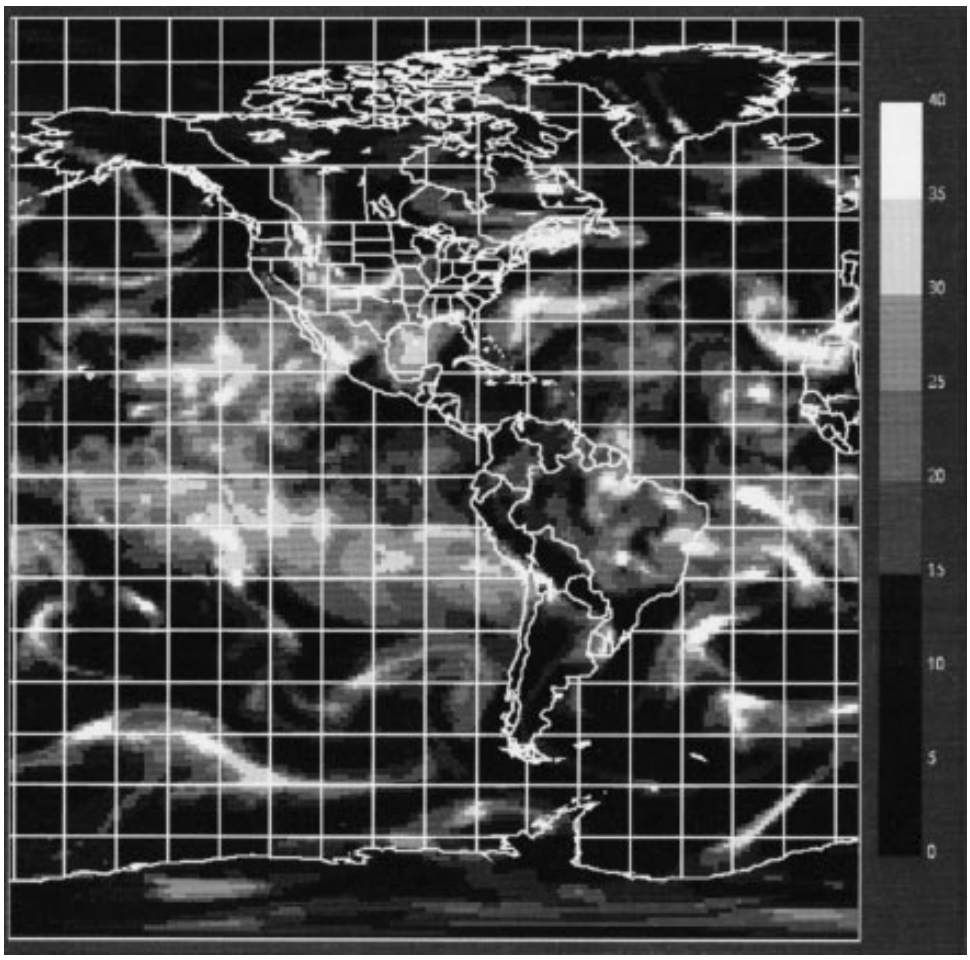

FIG. 2. (*Continued*)

reach 12 K. The CMC original forecast with 21 sigma levels was interpolated to 42 standard pressure levels. Linear fits were derived for 11 of these levels; 150, 200, 250, 300, 350, 400, 430, 475, 500, 570, and 620 mb. All DPD values were used in the fits except those corresponding to a surface pressure higher than 700 mb where the surface term in (1) may be nonnegligible and those corresponding to DPD $>$ 40 K, which are rare and may be spurious (excessively low values occasionally occur in the transformation from the spectral to the physical domain). The number of samples used in fits were in the approximate range 13 000 (T4) to 29 000 (T1).

Figure 3 shows 400-mb examples of fits for two extreme situations: nadir viewing in the Tropics (T1) and 70° viewing in Arctic air mass (T4). The raw scatterplot is shown on the left, and the linear fit derived from these data is on the right. Asterisks on the right represent 2-K BT bins of data on the left. It is seen that asterisks follow closely the fitting line over the entire range of BT even for the T4 air mass where the correlation ($r = 0.71$) appears and is indeed weaker than for the T1 air mass ($r = 0.86$). The DPD rms errors are 4.5 K for T1 (11.6% in terms of RH) and slightly lower at 3.9 K (but 12.5% in terms of RH) for T4 due to the fact that the range of possible DPD values shrinks as temperature decreases. The scatter of about 12% in RH is higher than the 10% scatter obtained by SB96 simply because the relationships are developed for specific pressure levels. As alluded to previously, DPDs in the range 30–40-K DPD (RH of 1%–3%) are relatively common in the Tropics, whereas most radiosondes do not report values above 30 K. It is for that reason that CMC analyses of DPD do not exceed 30 K, which translates into BTs not exceeding 255 K, while measurements up to 262 K are occasionally observed. Figure 3 also indicates a lower minimum in the fits of the order of 3 K; the exact value is the saturation DPD with respect to water phase at the mean (400 mb in this case) temperature of the data used in the fit.

Table 1a shows the DPD rms error for nine levels and for nadir and 70° viewing angles. Table 1b gives the corresponding correlation coefficient r. Formally these values are defined by

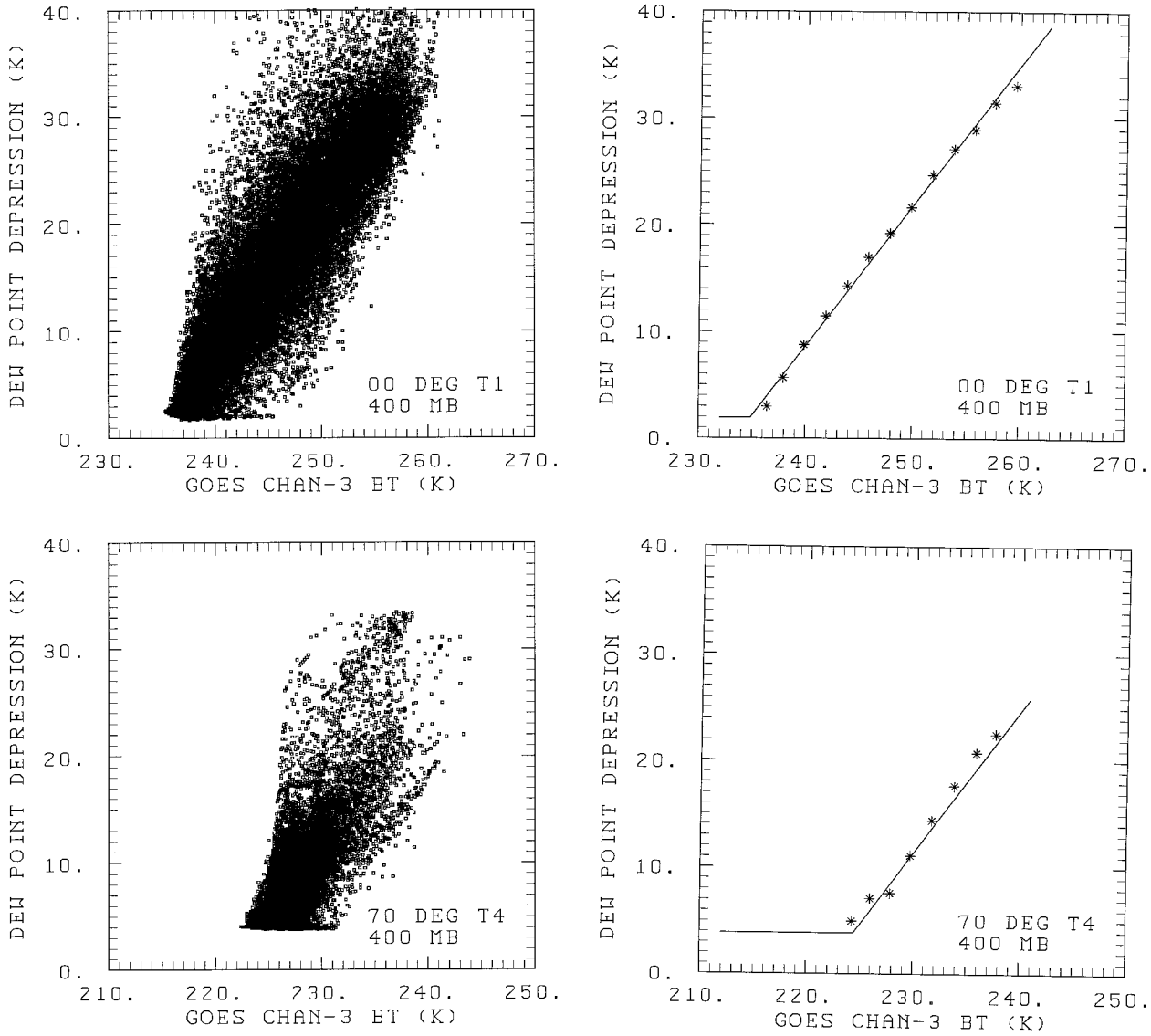

FIG. 3. (a) Scatterplot of 400-mb DPD at nadir for T1 air mass as a function of calculated BT. (b) Fitting line through all data in (a) with slope 1.3146, intercept −306.84. Asterisks represent 2-K BT bins from data in (a); horizontal line is minimum DPD defined as saturation value with respect to water phase at mean 400-mb temperature. (c) Same as in (a) but for 70° viewing angle and T4 air mass; (d) as in (b) but corresponding to data in (c) with slope 1.3436, intercept −297.71.

$$\text{rms}\,(\text{DPD}) = \left[\frac{\sum\,(\text{DPD}_i - a - b\text{BT}_i)^2}{N}\right]^{1/2} \tag{3}$$

$$r = \frac{\sum\,(\text{DPD}_i - \overline{\text{DPD}})(\text{BT}_i - \overline{\text{BT}})}{\left[\sum\,(\text{DPD}_i - \overline{\text{DPD}})^2 \sum\,(\text{BT}_i - \overline{\text{BT}})^2\right]^{1/2}}, \tag{4}$$

where $i = 1$, N and a and b are the intercept and slope of the linear regression. The correlation coefficient best indicates the level of maximum response. In the Tropics (T1), this level is 250 or 300 mb with correlation reaching or exceeding 90%; in very cold air masses (T4), the peak response is lower at 500 or 570 mb. Our evaluation is that fits with correlation coefficient exceeding 0.65 provide useful data in that the associated error is equal or lower to that of the guess field (typically 5–6 K for 300–500 mb). In the Tropics, data are then useful from 150 to 500 mb. CMC DPD analyses that stop at 300 mb could therefore be improved at levels 150–250 mb in the Tropics. For the T4 air mass, however, data appear useful only at levels 400–600 mb. The fitting parameters for the 16 fits times 11 levels are too numerous to list here. It is worth noting that the slopes are typically in the range 1–1.5, corresponding to the increment in DPD per degree increment in BT. Since observations are as-

TABLE 2. Retrieved 200–500-mb DPD (K) for BT = 240 K, air masses T1 and T4, and angles 0°, 39°, 56°, 70°.

Level		200	300	400	500
T1	0°	7.2	7.0	8.7	9.7
	39°	8.9	9.4	11.2	11.9
	56°	11.2	12.6	14.3	14.7
	70°	14.8	17.4	18.7	18.4
T4	0°	13.4	13.9	16.3	16.9
	39°	13.8	15.8	18.9	19.9
	56°	15.9	17.5	20.9	22.0
	70°	19.0	20.8	24.8	25.8

sumed precise to within 0.2 K (0.27 K for *GOES-8* and 0.15 K for *GOES-9* at 230 K), the resulting error on DPD due solely to the observation error is about 0.3 K, which is small in comparison to the error resulting from the fits (also the averaging of BT within a $1° \times 1°$ box further reduces the noise). The effect of undetected cloud is difficult to quantify: The presence of clouds lowers BT, which results in a wetter estimate than if only the clear portion of the 100-km area had been used. On the other hand, the desired quantity is the average humidity within the 100-km area. The likelihood of undetected cirrus is minimized in quality-control procedures defined in section 4.

Table 2 shows an example of DPD profiles for BT = 240 K, air masses T1 and T4, and the four viewing angles used in fits. Clearly, both dependencies in viewing angle and air mass are important. The profiles are smooth in the vertical with DPDs tending to decrease with height, a climatological behavior confirmed by radiosonde measurements (see GA93). For a given BT, viewing angle and T_{400}, the proposed solution is always the same; more complex vertical structures can only be obtained by additional channels with low inter-correlation and with information peaking at different heights. Simple vertical DPD structures such as those suggested by the retrievals are, however, typical in cloudless atmospheres and this plays a fundamental role in the success of the technique.

d. Evaluation on independent data

1) DPD

The DPD retrieval technique can be evaluated on independent data simulating the eventual application. Brightness temperatures that would be observed from *GOES-8* were calculated from the analysis valid at 0600 UTC 26 January 1996 (which was not influenced by Humsat data). These BTs were then used in the retrieval technique along with the corresponding viewing angle and 400-mb temperature to evaluate how close the retrieval algorithm can recover the DPDs of the analysis used here as ''truth.'' Table 3 shows the results for three levels (300, 400, 500 mb) and for air masses T1, T2, and T3 (there are not enough T4 data seen from a GOES disk) for cases without clouds above 700 mb. The errors

TABLE 3. DPD retrieval errors (rms, K) at as a function of level and air mass using BTs calculated from 0600 UTC 26 January 1996 analysis within the *GOES-8* disk. These errors can be compared with those in Table 1a except that all viewing angles are pooled together.

Level	300	400	500
T1	4.6	4.8	6.8
T2	3.5	4.5	6.3
T3	3.1	3.8	4.9

are similar to those seen in Table 1a, but tend to be higher by a few tenths of a degree. Considering errors of the radiative transfer model, errors introduced in the interpolation in viewing angle and T_{400}, and errors in GOES observations, the errors suggested in Table 1 should be slightly increased. As discussed further, a 1.25 multiplicative factor was used in assimilations for the DPD errors listed in Table 1.

2) BT

So far, only synthetic BTs have been discussed. For the same 26 January case, the calculated BTs were compared to the observed *GOES-8* BTs for the 3940 points where no clouds are seen by the Humsat system above 700 mb (including then potential cases with undetected clouds). Figure 4 shows the scatterplots for four different BT estimates: ANAL refers to BTs computed from the analysis; RET1 is as ANAL except that retrieved DPDs from the observed BT replace ANAL DPDs at all levels (150–620 mb) where the correlation coefficient exceeds 0.65; RET2 is as RET1 except that no retrievals are used above 300 mb; and RET3 is as RET2 except that the DPD estimates are limited to 30 K. The results indicate that the model differs from the observed BT by about 4.6 K rms with a -1.5-K bias. Brightness temperatures are limited to 255 K because of the lack of dynamic range in CMC analyses, that is, the 30-K DPD limit. The basic retrieval (RET1), on the other hand, is remarkably close to the observation with a rms of 0.62 K and a small bias. Clearly, the retrieval technique provides DPD estimates that reproduce the observed radiance used in their derivation very well. Also, and more importantly, the radiative transfer model reproduces real observations quite well. Results very similar to these were obtained on all cases examined. The RET1 result also suggests that errors in the input temperature profile have a relatively small impact on BT since the humidity retrieval alone reproduces observed BTs very well; a corollary is that the humidity signal in BT is well separated from the temperature signal from the division into air masses. RET2 results show that a significant portion of the BT signal comes from levels above 300 mb since the rms degrades to 1.8 K. Finally, RET3 results confirm what was seen in ANAL, that observed BTs above 256 K cannot be obtained if DPDs are limited to 30 K. This particular example was one of unusually large areas of observations

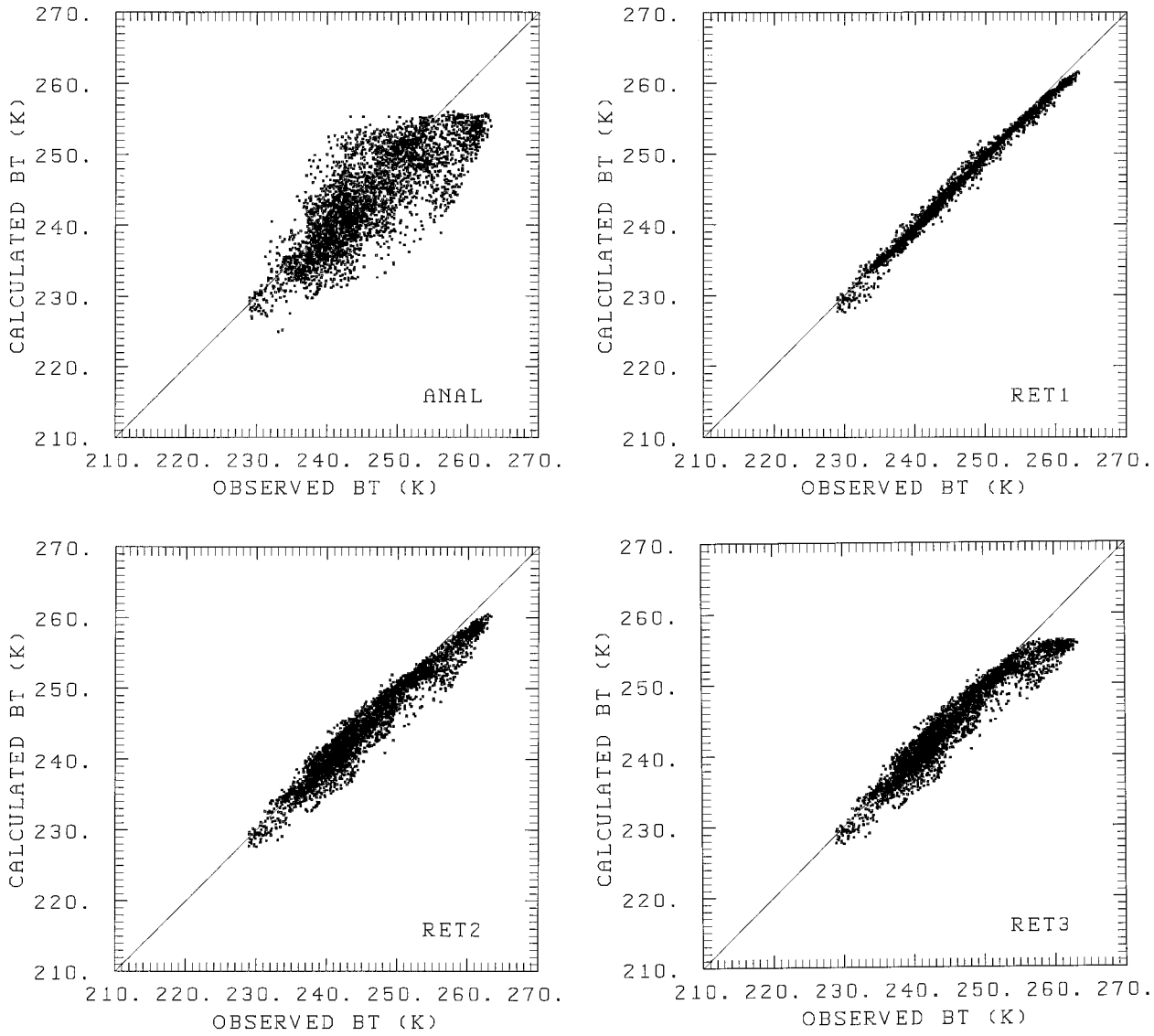

FIG. 4. Calculated versus observed *GOES-8* BT for analysis of 26 January 1996 at 0600 UTC; (a) from unmodified analysis (ANAL, rms: 4.60 K, bias: −1.54 K, *r*: 0.812); (b) from retrieved DPD replacing ANAL DPDs where fits have a correlation higher than 65% (RET1, rms: 0.62 K, bias: 0.05 K, *r*: 0.997); (c) as RET1 except that only retrievals 300 mb and below are used (RET2, rms: 1.79 K, bias: −0.42 K, *r*: 0.972); (d) as RET2 except that DPD estimates are limited to 30 K (RET3, rms: 2.22 K, bias: −0.68 K, *r*: 0.961).

exceeding 255 K and shows the strong BT response at low humidities (see Blackwell and McGuirk 1996).

e. BT bias correction

As just shown, the technique provides DPD estimates that reproduce the observed BTs to good accuracy with no *apparent* bias. It is very important to get a bias as small as possible since the slopes of the linear fits are typically in the range 1.0–1.5, which implies DPDs off by the product of the slope times the bias *over the entire DPD range and at all levels.* In parallel runs, it was found that the SAT BT bias (computed minus observed from analyses and forecasts with Humsat data) was small, but that the forecast model without Humsat data (NOSAT) apparently had a negative bias of about 1.3 K (as seen from *GOES-8* and *GOES-9* disks over clear areas; Fig. 4a is an example of that). On the other hand, 6-h SAT forecasts had a dry DPD bias with respect to radiosondes of about 1.0–2.0 K for several weekly periods, while the NOSAT forecasts had little bias. Reconciliation of those two ''truths,'' observed BT from satellite and DPD from radiosondes (known to be imperfect but we assume here for the moment that the bias over a long period is small), could only be achieved by assuming that it was the NOSAT forecasts that had no

significant bias, while the Humsat data were too dry and caused a BT bias of about 1.3 K from fits based on a RTM having a −1.3-K bias. The solution was to reduce DPDs by 1.3 times the slope of the original relationships and to add 1.3 K to BT RTM calculations for comparisons with GOES observations. In subsequent assimilation periods the DPD bias in 6-h SAT forecasts were small. The same adjustment was done for both satellites. A line-by-line radiative transfer model was applied to standard atmospheres, taking into account the detailed response functions of each satellite. Results indicated that the BT differences between *GOES-8* and *GOES-9* were negligibly small (< 0.1 K; D. S. Turner 1996, personal communication). In the late stage of this research, we looked for an independent confirmation of the 1.3-K bias. We used an ensemble of 1103 globally representative profiles for which *GOES-8* channel 3 BTs were calculated using a line-by-line model. Comparison with the fast radiative transfer model used in this study confirmed a BT bias of 1.1 K and an rms difference of 0.27 K, which is satisfying. Also, the BT bias differences were systematically between 0.8 and 1.4 K over the entire range of values, suggesting that a simple constant bias adjustment for all BTs is justified to first order.

f. Cloudy retrievals

This section briefly describes the cloudy estimates that complement the UTH clear sky estimates described so far. The Humsat system (GA93) was built to provide humidity estimates in all cloud conditions at the scale of 100 km. The statistical DPD estimates vary with cloud class and different estimates are provided for latitudes above and below 30°. The wettest profile is that of the deep cumulonimbus class identified by a cloud top above 150 mb; a strong weight, similar to that of radiosonde, is given to estimates of that class in the analysis, which improves the analysis in precipitation areas such as the intertropical convergence zone (ITCZ). In the case of clouds present above 700 mb, the 300–500-mb Humsat DPD estimates vary between about 3.5 and 12 K. In these situations (excluding the cumulonimbus class), the 300–500-mb estimate based on cloud class is now averaged with the estimate based on DPD–BT fits (equal weight of 0.5 to each estimate), thereby giving some BT dependence on the estimates. Thus, cold/warm BTs will make the final estimate wetter/drier than the estimate based on cloud classification. It was found that DPD histograms similar to those of the model (NOSAT analyses and forecasts) were obtained in that manner, except for values near saturation (< 2.5 K), which are not generated by the Humsat system at UTH levels. As seen later in the text, a quality-control procedure rejects Humsat estimates from classes affected by clouds whenever the 6-h forecast DPD is wetter than the Humsat DPD estimate, precisely to compensate for the lack of satellite-inferred near-saturation values. Therefore, the role of the cloudy-sky estimates is essentially that of correcting the analysis in regions where the first guess appears too dry. Preciseness in those cases, if desirable, is less critical inasmuch as the estimates correct the analysis in the right direction.

3. Error correlations

a. Horizontal

At the CMC, the humidity analysis is univariate and the variable analyzed is DPD. The analysis **A** is a correction to a background field **B,** which is a 6-h forecast, via the equation

$$\mathbf{A} = \mathbf{B} + \sum W_i f_i, \tag{5}$$

with $f_i = O_i - B_i$, where i is the site of observations O_i, and W_i is the weight to be given to each difference f_i (called innovation). As described in Daley (1991), the classical linear system solved in most NWP centers for the weights W is

$$\sum_{j=1,N} \left(\mu_{ij} + \nu_{ij} \frac{\sigma_i \sigma_j}{\sigma_b^2} \right) W_j = \mu_{ai}, \tag{6}$$

where μ_{ij} is the horizontal correlation of background errors between sites i and j, and ν_{ij} is the horizontal correlation of observation errors; σ_i is the observation error at site i and σ_b is the background error, assumed constant around an analysis grid point at location a. For the humidity variable, the horizontal correlation of errors, both for the background and Humsat estimates, is modeled by the function

$$\mu_{ij} = \left(1 + \frac{D_{ij}}{L} \right) \exp\left(-\frac{D_{ij}}{L} \right), \tag{7}$$

where D_{ij} is the distance between a pair of estimates and L is a length scale to be determined by a fit. At distance L, one notes that the correlation has dropped to 0.74. A good deal of work is required to obtain the background length scales L_b (see Mitchell et al. 1990). In practice, L_b and σ_b vary with pressure level in several latitude bands for the winter and summer season. Large amounts of collocated radiosondes and 6-h forecasts are binned by distance, and the zero intercept of the horizontal covariance fit determines σ_b. As models evolve, error statistics are recalculated periodically.

For Humsat correlations, radiosondes in Europe were used as it is where the radiosonde network is the most dense, in collocation with Meteosat-derived Humsat profiles using the GA93 dataset (see Garand 1994). Error covariances were binned in about 200-km distance bins and there was several thousand pairs in each bin. We found that Humsat observation pairs can be divided into two groups: WET designates pairs where the sum of dewpoint depression estimates is below 12 K, DRY designates pairs where it exceeds that threshold. Also, no significant correlation was found between estimates differing by more than 3 K. Table 1 shows the DRY

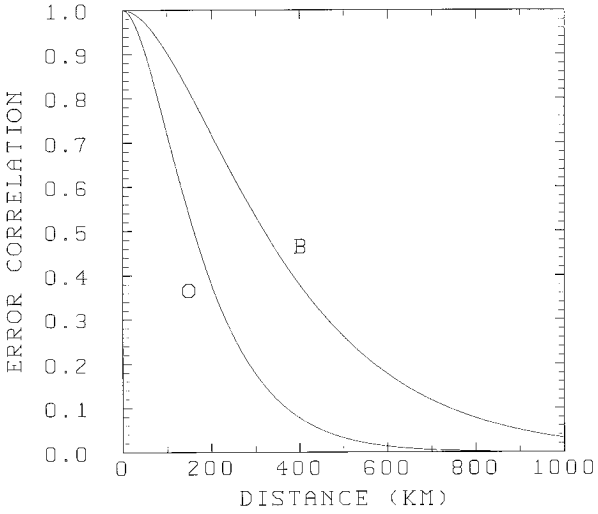

FIG. 5. DPD background (*B*) and Humsat (*O*) error correlation as a function of distance at 300 mb as estimated from Eq. (4) with L_o = 95 km and L_b = 190 km.

and WET estimates of L_o as well as values of L_b established in the northern midlatitudes in winter (L_o presented here is to be used independently of latitude and season). No attempt was made to recompute these length scales from the revised Humsat system described in this paper; differences in L_o between the new and revised system are expected to lie within the error margin of the estimates (about 20%) since there has been little change to low-level estimates, while upper-level estimates are again based on DPD versus BT fits. Figure 5 shows the 300-mb Humsat and background error correlation as a function of distance. As one would expect, length scales are smaller for WET than for DRY data for most levels.

The importance of considering the horizontal correlation of errors has been recognized for height and temperature retrievals derived from satellites (Sullivan 1993). The importance for humidity estimates is also evident. Without this effect included, the weight of the data is strongly influenced by the density of data, whereas a reasonable weight proportional to the quality of the estimates is obtained regardless of the density of data with the effect considered (Garand 1994; it was also showed that for the same background and observation rms error, the observation has more weight on the resulting analysis than the background when $L_b > L_o$). The effect can be neglected only if the distance between estimates exceeds 4*L*. Experience showed that having errors of the order of 20% on L_o is acceptable; by far it is preferable to use imperfect L_o estimates than to neglect the correlation altogether. Technically, care must be taken to compute horizontal correlations only within limited volumes in order to maintain the cost of these calculations at a minimum. This problem currently represents a challenge in the 3D variational analysis system soon to replace the optimum interpolation system.

TABLE 4. Values of length scales L_o (km) for horizontal correlation of Humsat errors for dry and wet pairs. Northern midlatitude winter background values L_b also shown.

Level	L_o (dry)	L_o (wet)	L_b
1000	122	147	212
925	139	121	190
850	156	96	168
700	151	108	123
500	128	106	127
400	108	87	133
300	95	96	190

b. Vertical

With the same dataset as in the previous section, it was straightforward to compute vertical error correlations. In that case, all data were used (no wet–dry distinction). The result is shown in Table 5. The correlations are usually small two standard pressure levels away. In 3D analysis, the correlation is expressed as the product of the horizontal and vertical error correlations.

4. Quality control

Quality control in the present context aims at identifying data that could cause errors in the analysis and therefore that should preferably not be used. At the levels under study here (300–500 mb), four criteria of rejection are used.

1) Cirrus clouds. When clouds are detected above 400 mb and when at the same time the model is wet at 400 mb (wet being identified by DPD < 8) but dry at 700 mb (DPD > 12), then there is a good chance that the situation is that of cirrus (detected by both the model and satellite) overriding a dry lower atmosphere. In that situation the 500-mb estimate (wet) is not used. This situation is typical ahead of low pressure systems or warm fronts.
2) Regions near saturation. Humsat estimates are rarely below 3-K DPD. In regions where Humsat estimates are moist (< 10 K) but less moist than the first guess, the data are not used. This occurs mostly in frontal situations, in convective areas, and in moisture convergence zones in general. This criterion is important

TABLE 5. Vertical correlation of Humsat error estimates.

Level	1000	925	850	700	500	400	300
1000	1	0.61	0.25	0.11	0.09	0.08	0.13
925		1	0.59	0.20	0.10	0.10	0.14
850			1	0.28	0.10	0.14	0.15
700				1	0.23	0.12	0.10
500					1	0.53	0.25
400						1	0.47

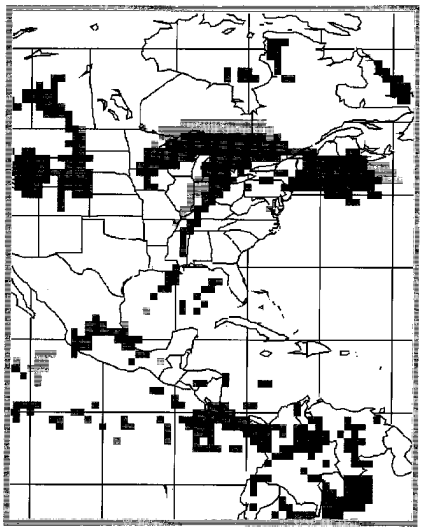

FIG. 6. Example of 500-mb quality control for a *GOES-8* scene at 2345 UTC 29 April 1996. Gray areas are rejected by the cirrus criterion and black areas by the near-saturation criterion. White areas passed quality control.

because areas near saturation play an important role in generating realistic precipitation early in the forecast; also, these regions are associated with minima of outgoing radiance. From this criterion, moist Humsat estimates can only have a moistening effect, in particular in regions of strong disagreement with the first guess. Most rejected data are due to this criterion.

3) Low surface pressure. When the surface pressure is lower than 700 mb, 500-mb Humsat estimates are not used. This occurs over a portion of the Andes and over the highest peaks of the Rockies.
4) Near-isothermal atmosphere. When visible data are not used and when the 600-mb temperature of the guess field is warmer than that of the ground minus 10 K, the situation is judged difficult (near isothermal) for cloud thresholding and 500-mb data are not used. This criterion occurs mostly in Arctic air masses.

Figure 6 shows a map of quality control at 500 mb for a particular case seen by *GOES-8*. The near-saturation rejected region over the Great Lakes corresponds to a frontal system easily recognizable by its comma shape; the cirrus rejection criterion is active ahead of that system in a sector where indeed there is a good chance that the high clouds are over a drier lower atmosphere. Missing lines and noisy lines (not seen in Fig. 6) are identified from the raw data and are not processed.

For completeness, quality-control procedures applied to lower levels (1000–700 mb) can briefly be mentioned since Humsat data at these levels are to be used over oceans in assimilation cycles (and operationally). Criteria 2, 3, and 4 above apply also at low levels. Low-level data are rejected if the integrated water vapor differs from the guess equivalent by more than 2.5 times the expected error on that quantity (as defined in Deblonde et al. 1995). Clear-air low-level statistical estimates lack dynamic range as they simply represent the mean clear-sky value; these estimates are rejected whenever the guess estimate is drier. About 80% of the available data are used at levels 300–500 mb. The percentage drops to about 40% at 700 mb and to 15% at 1000 mb.

5. Impact on analyses and forecasts

a. System configuration

The parallel analysis and forecast systems, ran between mid-February to mid-April 1996, differed only from the use (SAT) or nonuse (NOSAT) of Humsat DPD estimates. Satellite-derived temperatures (mostly higher levels) are used operationally (NOSAT) but no satellite humidity enters into the analysis (only conventional data from radiosondes or ground observations). *GOES-8* and *GOES-9* data were used in the analysis without overlap, that is, *GOES-8* provides data east of 105°W and *GOES-9* provides data west of that longitude. While data are extracted on a $1° \times 1°$ grid and were used at that resolution with *GOES-7*, only one of two samples in each direction are sent to the analysis in this new configuration, thereby reducing the horizontal resolution to about 200 km. The estimates originate from about 5500 sites from 60°N to 60°S and from 165°E to 15°W (70° is the limit for the satellite-viewing angle). The additional cost to the total analysis time was a modest 8%, but the decision was nevertheless taken to postpone the use of full-resolution data until a more powerful computer becomes available because other types of satellite data are soon to be tested in parallel runs that will further add to the analysis time. The advantage of full resolution is most apparent in sectors of scattered cumulonimbus and in relatively narrow dry regions behind cold fronts. Estimates at 300, 400, and 500 mb are used over land, while over water 700–1000 mb are also used in the same manner as in GA93. This choice is motivated by the fact that cloud analysis is more reliable over ocean due to the uniform background; also, much more data are available over land, which directly or indirectly contribute to the humidity analysis.

The error associated with the 300–500-mb clear-air estimates is that suggested by the fits (Table 1a) times an amplification factor of 1.25. That factor is also applied to cloudy estimates, excluding the cumulonimbus class. The amplification factor is justified by the application to independent data; it gave optimum results in short-term DPD forecasts as verified from radiosondes (discussed in section 5c). Background errors do not depend on cloud conditions; for UTH levels they are in the range 5.7–6.1 K in the Tropics and Southern Hemisphere and in the range 4.9–5.5 K north of 30°N. At

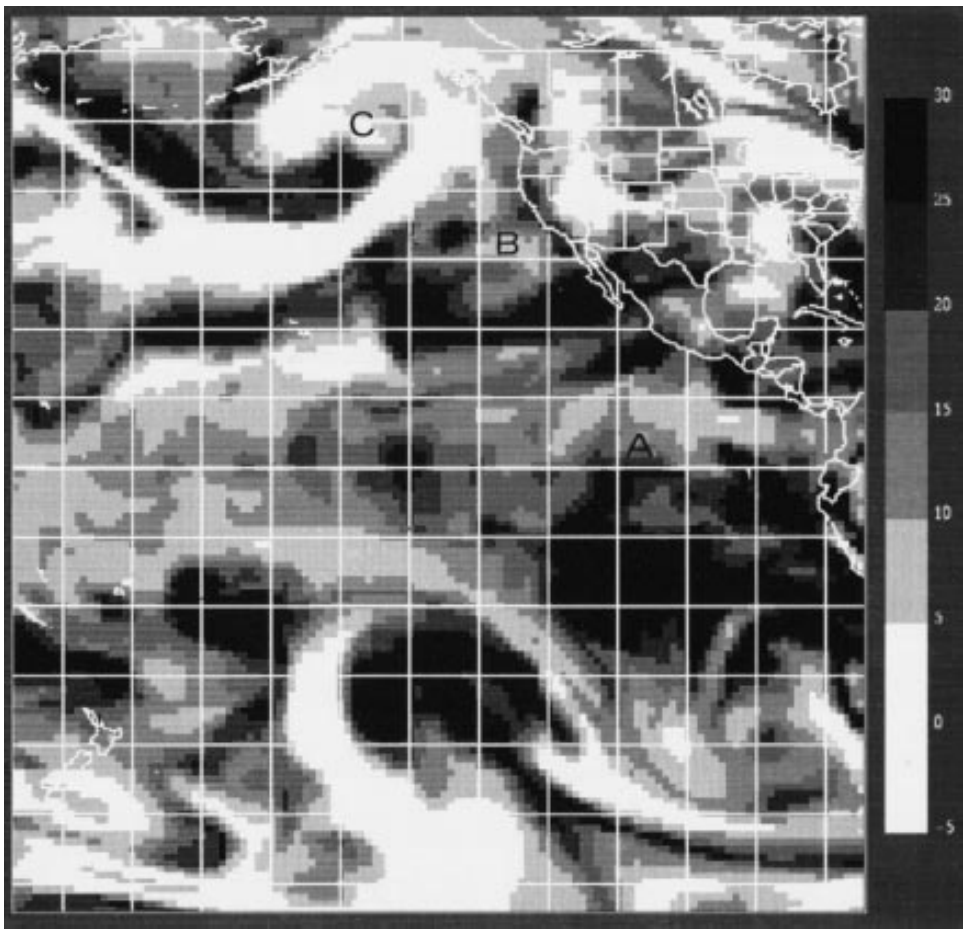

FIG. 7. Example of 500-mb DPD in NOSAT (a) and SAT (b) analysis for 4 April 1996 at 0000 UTC; (c) difference SAT minus NOSAT; (d) observed GOES-9 BT. Areas for comparisons denoted by A, B, and C in (a) and (b) are referred to in the text.

lower levels, errors vary between 3.0 and 5.5 K with the lowest values at 1000 mb.

b. Subjective evaluation

Parallel assimilation cycles and 0–48-h forecasts launched at 0000 UTC from these different cycles were intercompared by meteorologists for 2 months. Regions of maximum differences were evaluated subjectively from comparisons with visible, infrared, and water vapor satellite images. Figure 7 provides an example of differences between SAT and NOSAT DPD analyses at 500 mb along with corresponding observations of 6.7-μm BT from *GOES-9.* At first sight, the analyses appear quite similar because they are dominated by the major disturbances represented by wet (white) areas. However, Fig. 7c shows DPD differences as large as 20 K. Closer inspection reveals a better correspondence between SAT analyses and BT observations. In particular, the wet areas in the tropical band 10°S–20°N match significantly better (in the region denoted by A, for instance). The same is true for dry (dark) areas just west of California (B) and east of the head of the major comma cloud observed south of Alaska (C). This better correspondence is to be expected since the satellite data enter into the analysis, and is the result of using both clear-sky measurements derived from water vapor radiances and cloudy-sky estimates derived from cloud classification.

Other means of evaluation included collocation of vertical profiles with radiosondes and appreciation of 0–12-h forecast accumulated or instantaneous precipitation using ground observations and satellite images (not shown). The ITCZ was better depicted in the SAT analyses and the 0–12-h precipitation originating from major cumulonimbus clusters was also judged superior. However, small-scale convection from isolated cumulonimbus did not appear improved in SAT analyses, in part because only one of two $1° \times 1°$ box was used. Over oceans, low-level moisture (850–700 mb) was also evaluated; regions of extended stratocumulus were clearly superior in SAT analyses and

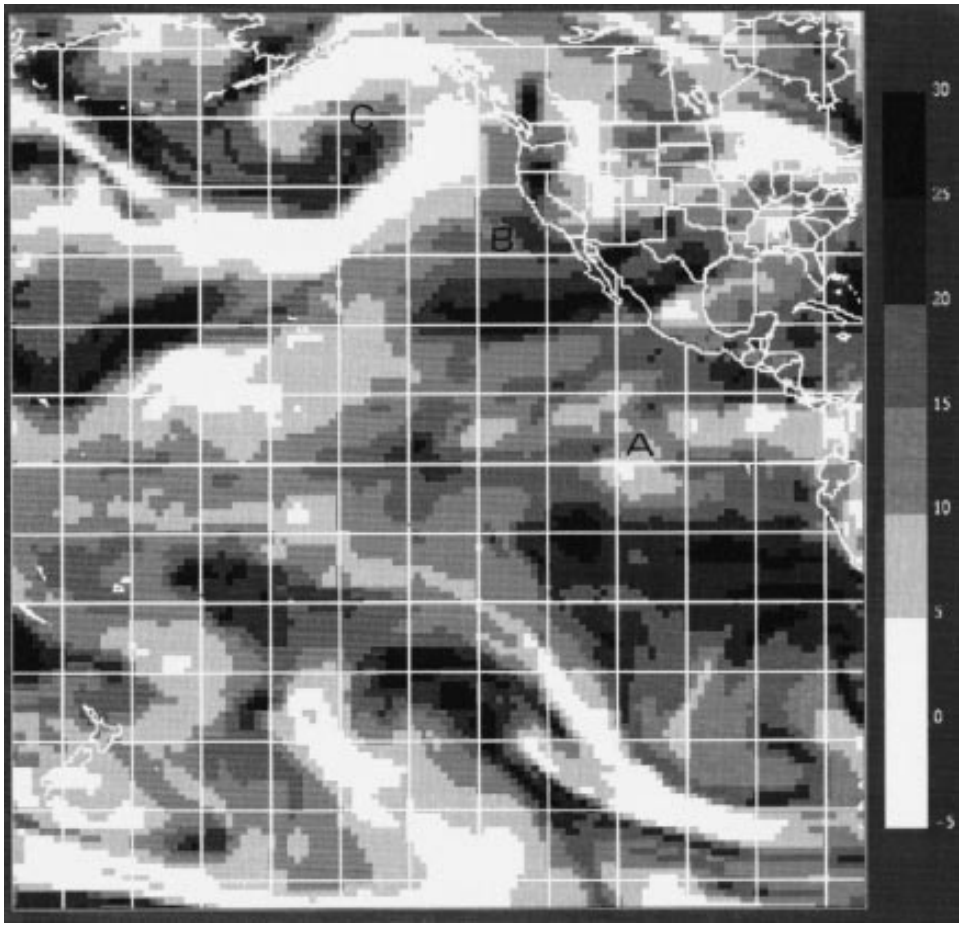

FIG. 7. (*Continued*)

short-term forecasts. A common observation was that the Humsat data often did not appear to influence enough the analysis. Indeed, their weight is typically similar or slightly less than that of the background. Consequently, in rapidly moving systems, the corrections are often not as strong as would be desirable. CMC meteorologists judged that the Humsat system alleviated considerably the need for manual humidity bogus over the oceans (DPD corrections judged from satellite imagery), but it did not eliminate it completely. The question of relative weight between the background and the data is complex. The weight of the background is derived from collocations with radiosonde over continents and it is invariant with location (presumably it should be reduced over oceans) and with the synoptic situation, whereas the weight of the satellite data does depend either on the cloud class or, in the case of DPD–BT fits, on the viewing angle and on the air mass. It would be preferable to work with satellite to background error ratios if those could be derived as a function of cloud or airmass conditions.

c. Objective evaluation

1) COMPARISONS OF ANALYSES AND FORECASTS WITH RADIOSONDES

Analyses and 6-h forecasts that serve as background field were evaluated in terms of DPD difference with radiosondes by interpolation of analyzed DPD fields to the radiosonde sites. Since radiosonde observations are available at 0000 and 1200 UTC, the evaluations are those valid at those times and the 6-h forecasts those emitted at 0600 and 1800 UTC. It was found that for radiosondes over North America (about 90 sites) as well as for the few (about 18) available over Mexico and the Caribbean islands, SAT and NOSAT statistics were very similar in terms of winds and geopotential. For the variable of interest, DPD, there was a modest but consistent improvement at upper-tropospheric levels. Table 6 shows the results for two assimilations periods over North America. The global model assimilation (2–10 April) and the regional model assimilation (11–19 April) were the last done before implementation. Results at lower levels (1000–850 mb) are not shown because the

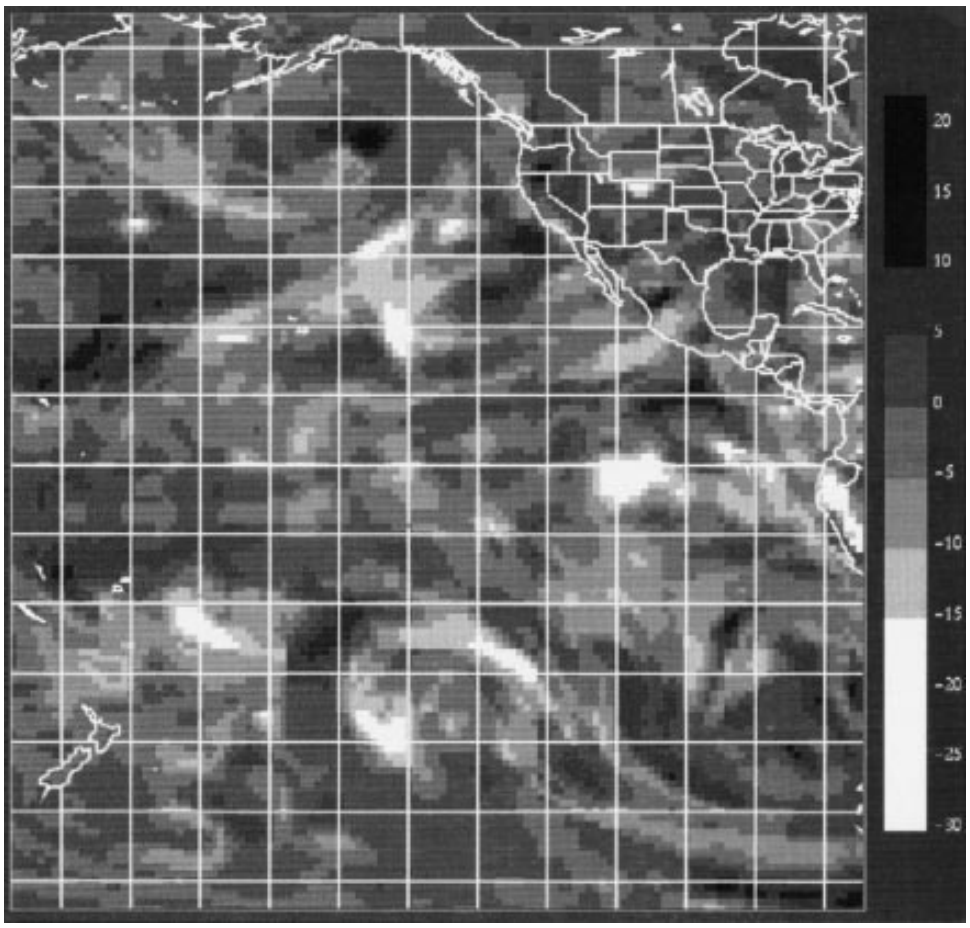

FIG. 7. (*Continued*)

differences are negligibly small since only 300–500-mb data are used over land. Only rms differences are given, biases were small, of the order of a few tenths of a degree. Humsat data increase significantly the rms $A - O$ (bias included) between the analysis (A) and radiosonde (O) observations, by 0.2–0.5-K rms. This is to be expected since Humsat data are competing with radiosonde data to produce the analysis. However, in subsequent 6-h forecasts the proximity to radiosondes $B - O$ (B for background or 6-h forecast) is either equal or improved by a few tenths of a degree in comparison with NOSAT forecasts. Results for Mexico and the Caribbean islands (not shown) were similar and there was one weekly period in late March where the SAT DPD forecasts were improved by as much as 1.0 K at 300–500 mb.

Forecasts up to 48 h were also evaluated with respect to radiosondes over North America. Differences tended to be small, to slowly increase with time, and to favor SAT forecasts. Figure 8 shows rms differences in temperature, DPD, and height of 48-h forecasts. The temperature bias is also shown. These results represent an ensemble of seven forecasts launched at 0000 UTC on consecutive days in early April 1996 (over 600 collocations). The improvement on height is of the order of 0.8 m from 700 to 300 mb. DPDs are improved over most of the atmosphere, in particular in the layer 250–400 K where the improvement is of the order of 0.2–0.4 K. Temperature improvement is at most 0.1 K but the bias is lower by about 0.25 K between 250 and 400 mb. Lower than 500 mb, the temperature bias is larger in SAT forecasts by 0.1 K. This may be related to the fact that in that period, precipitation appeared to be slightly less in SAT than in NOSAT forecasts (less latent heating). Objectively, it was noted from DPD histograms that NOSAT analyses had higher occurrences of 0–2-K DPD. Perhaps the protection of regions near saturation by quality control (Fig. 5) should be enlarged by a few 1° pixels since dry estimates very next to wet regions where satellite data are not used will have a drying influence on the wet sector.

2) BRIGHTNESS TEMPERATURE COMPARISONS

Over oceans, objective evaluations are difficult because of the lack of in situ data. Comparisons of fore-

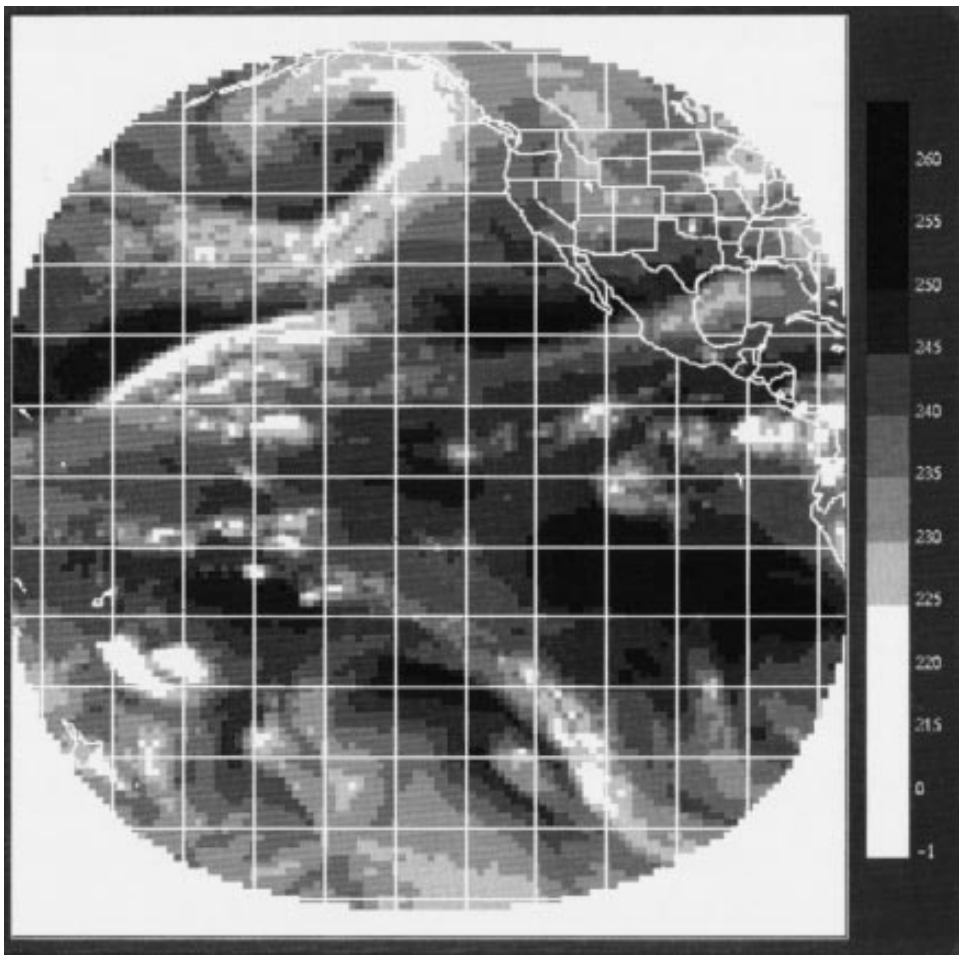

FIG. 7. (*Continued*)

casts with SSM/I derived integrated water path are possible but would be informative mostly on lower-tropospheric humidity. However, an objective evaluation of calculated versus observed BTs is possible everywhere; furthermore, it is most interesting to do this evaluation as a function of time into the forecast. Table 7 shows such an evaluation for SAT and NOSAT forecasts of 0000 UTC 4 April. We have noted earlier that basic DPD retrievals reproduce observed BTs to within 0.7 K. Table 7 shows that at initial time, the difference between observed and calculated BTs is close to 2.0 K. The gap between these numbers is the result of blending the estimates with the trial field. In addition, analyses are only carried out up to 300 mb, whereas the 0.7-K figure was based on data used possibly up to 150 mb. On the other hand, NOSAT analyses have a proximity to BT observations of about 4-K rms, significantly less than the SAT analyses. These three figures: 0.7 K (basic retrieval), 2.0 K (SAT analysis), and 4.0 K (NOSAT analysis) were very similar (to within 15%) in all cases studied. Table 7 reveals that the superiority in terms of 6.7-μm BT of SAT forecasts remains significant up to 24 h; the rms gradually increases to reach the NOSAT level at 36 or 48 h.

TABLE 6. DPD rms distance (K) to radiosonde observations of the analysis ($A - O$) and background (6-h forecast) fields ($B - O$) over North America in global and regional SAT and NOSAT assimiliation cycles.

	Global				Regional			
	NOSAT		SAT		NOSAT		SAT	
Level	$A-O$	$B-O$	$A-O$	$B-O$	$A-O$	$B-O$	$A-O$	$B-O$
300	2.08	5.38	2.48	5.13	1.71	4.88	2.16	4.91
400	2.06	5.24	2.59	4.93	1.96	5.81	2.35	5.55
500	2.35	5.61	2.90	5.69	2.33	5.96	2.55	5.75
700	2.66	5.63	2.74	5.69	2.50	5.85	2.46	5.74

One puzzling aspect of Table 7 is that the BT error in NOSAT analyses remains unchanged throughout the forecast. The explanation, we believe, is that the data in the table refer to large-scale dry areas slowly evolving in a 48-h period and well captured by the analyses. NOSAT analyses and forecasts are, however, clearly deficient in reproducing details in the BT pattern. In gen-

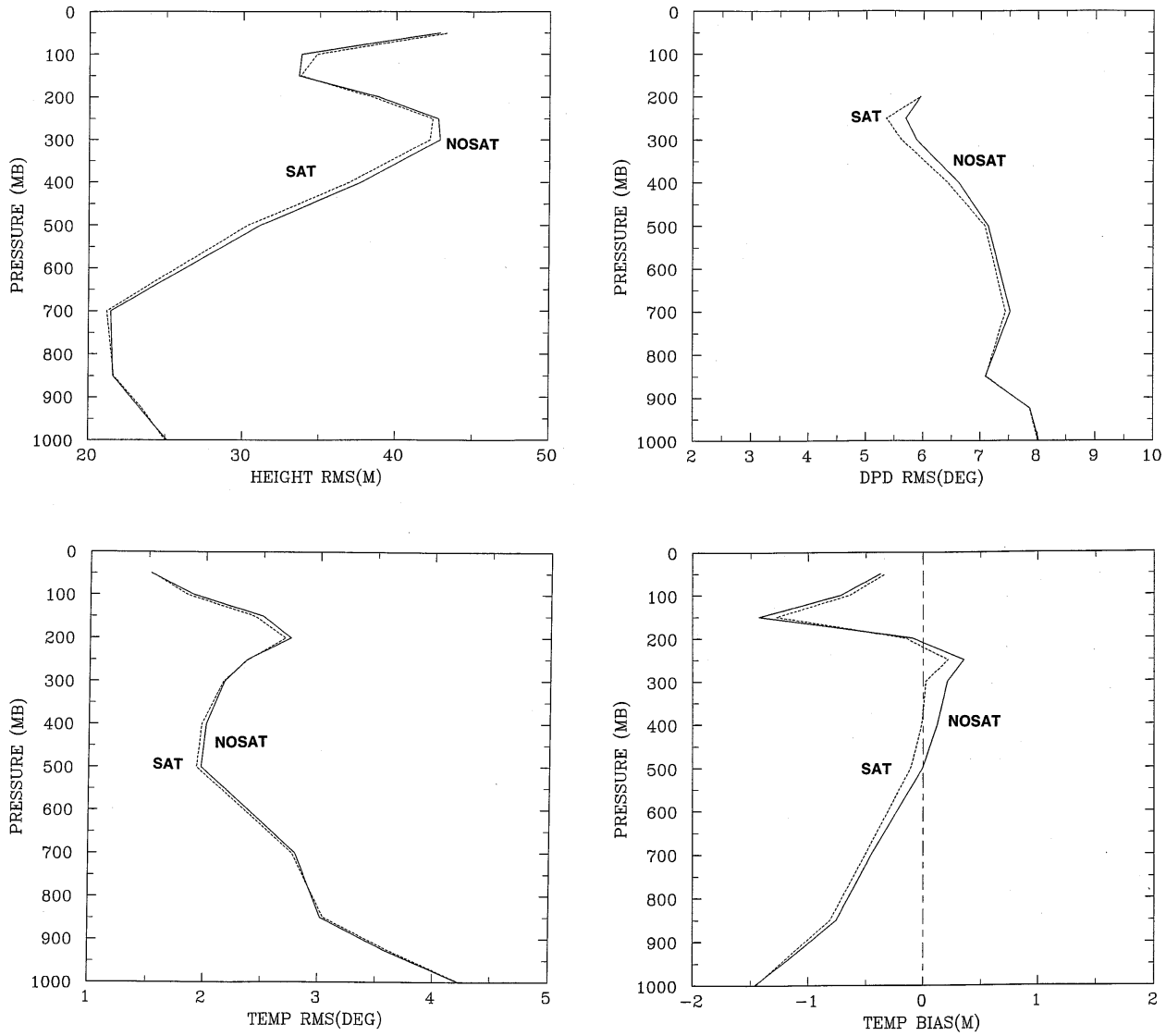

FIG. 8. Objective evaluation of SAT (dashed line) and NOSAT (full line) 48-h forecasts with respect to radiosondes for an ensemble of seven consecutive forecasts launched at 0000 UTC in early April 1996. (a) Height rms (m); (b) DPD rms (K); (c) temperature rms (K), and (d) temperature bias (K) as a function of pressure (mb).

eral, SAT fields are smoother than NOSAT fields; similarly, satellite BT observations are smoother than corresponding calculated NOSAT BTs.

Biases noted in Table 7 are small and of varying sign in the various *GOES-8* forecasts, giving confidence in our final bias adjustment. Biases for *GOES-9* in all NOSAT forecasts are in the range −0.8–1.3 K and would therefore appear as 1.3 K worse without the adjustment. The revised Humsat system was implemented operationally at the CMC in mid-April 1996.

6. Conclusions

A method to obtain upper-tropospheric humidity estimates at specific levels was developed for *GOES-8* and *GOES-9*. The technique is based on the linearity between DPD and 6.7-μm brightness temperature, and takes into account dependencies on satellite-viewing angle and airmass type in a manner equivalent to that of Soden and Bretherton (1996), the major difference being the application at specific levels. The estimates provided at the various levels are not independent as they all come from a single 6.7-μm BT measurement: a smooth profile is generated, typically characterized by a slight decrease of DPD with height. The humidity estimates can be assimilated in the same manner as radiosondes. Also, the technique is well suited for the processing of large amounts of water vapor images for climatic applications. In that respect, 400 mb is the level of maximum response on

TABLE 7. Proximity of forecast brightness temperature (rms, K) to *GOES-8* and *GOES-9* channel 3 observations as a function of time. Forecast of 0000 UTC 4 April 1996. Bias (forecast minus observed), correlation (r) and number of collocations (N) also shown. Collocations in regions without clouds above 700 mb. Only a half disk was available for *GOES-8* 6 h.

		NOSAT			SAT		
	N	Bias	rms	r	Bias	rms	r
(a) *GOES-8*							
00 h	4072	0.7	3.88	0.77	0.3	2.17	0.92
06 h	1775	0.8	3.75	0.78	0.3	2.32	0.91
12 h	3630	0.4	3.70	0.77	0.0	2.76	0.87
24 h	4265	−0.1	3.55	0.82	−0.5	3.20	0.85
36 h	3385	0.1	3.93	0.74	−0.5	3.48	0.79
48 h	3921	−0.1	4.02	0.76	−0.7	3.82	0.78
(b) *GOES-9*							
00 h	3719	−0.8	3.93	0.74	0.0	1.98	0.92
06 h	3312	−1.2	3.94	0.76	−0.4	2.36	0.90
12 h	2916	−1.1	4.14	0.72	−0.5	2.93	0.85
24 h	3495	−1.2	3.88	0.78	−1.1	3.68	0.80
36 h	2632	−1.3	3.98	0.77	−1.3	3.84	0.79
48 h	3465	−1.3	3.80	0.80	−1.5	3.98	0.79

a global basis (250–350 mb in the Tropics, 450–550 mb in polar regions).

The technique is now part of the Humsat system that in cloudy regions provides proxy data based on cloud classification. This combination of retrievals based on the physics of radiative transfer in clear air and on cloud analysis in cloudy situations attempts to make the most out of available information. Details on quality-control procedures and on the treatment of the correlation of observation errors were provided. The cloud and radiation parameters extracted at $1° \times 1°$ every 6 h from the Humsat system are archived and have been used on several occasions for model verification (e.g., Yu et al. 1997; Dastoor 1994).

The evaluation during parallel runs led to the implementation of this revised Humsat system. Subjective evaluation confirmed that SAT analyses and short-term forecasts fit more closely the patterns seen in satellite imagery. In particular, the ITCZ is better depicted. Objective evaluation with radiosonde over North America indicated a modest but positive impact on the mass field and upper-tropospheric humidity estimates. It was noted, however, that differences between SAT and NOSAT analyses and forecasts were much larger over ocean than over land where radiosondes are available. In terms of brightness temperature, SAT analyses were clearly superior to NOSAT ones (2 K versus 4 K), and that superiority was maintained up to 2 days. It was shown that the water vapor channel provides useful information well above the 300-mb level where most radiosondes cease to report. It was also emphasized that the artificial 30-K DPD maximum in humidity observations limits computed brightness temperatures to about 256 K while observations several degrees warmer do occur.

The technique could easily be adapted to water vapor imaging channels onboard Meteosat or GMS. It could also be extended to the three water vapor sounding channels of GOES, but in that case data are not available on full disks; for these radiances the direct assimilation by variational methods is the likely choice for the future through the minimization process involving all sounding channels. A comparison of the analysis increments provided by the two methods would be of interest.

Acknowledgments. The authors thank J.-G. Desmarais and his team of meteorologists who evaluated with great care the parallel runs for two months. We thank A. Alfheim for his help in the preparation of the GOES data, D. S. Turner for line-by-line calculations, G. Lemay for the evaluation of forecasts using radiosonde data, C. Chouinard for revising the text, and two anonymous reviewers for useful suggestions.

REFERENCES

Bates, J. J., X. Wu, and D. L. Jackson, 1996: Interannual variability of upper-tropospheric water vapor brightness temperature. *J. Climate,* **9,** 427–438.

Blackwell, K. G., and J. P. McGuirk, 1996: Tropical upper-tropospheric dry regions from TOVS and radiosondes. *J. Appl. Meteor.,* **35,** 464–481.

Daley, R., 1991: *Atmospheric Data Analysis.* Cambridge University Press, 457 pp.

Dastoor, A. P., 1994: Cloudiness parameterization and verification in a large-scale atmospheric model. *Tellus,* **46A,** 615–634.

Deblonde, G., L. Garand, P. Gauthier, and C. Grassotti, 1995: Assimilation of SSM/I and GOES humidity retrievals with a one-dimensional variational analysis scheme. *J. Appl. Meteor.,* **34,** 1536–1550.

Garand, L., 1983: Some improvements and complements to the infrared emissivity algorithm including a parameterization of the absorption in the continuum region. *J. Atmos. Sci.,* **40,** 230–244.

——, 1993: A pattern recognition technique for retrieving humidity profiles from Meteosat or GOES imagery. *J. Appl. Meteor.,* **32,** 1592–1607.

——, 1994: Assimilation of satellite humidity retrievals at the CMC. Preprints, *Seventh Conf. on Satellite Meteorology and Oceanography,* Monterey, CA, Amer. Meteor. Soc., 397–399.

Liou, K.-N., 1980: *An Introduction to Atmospheric Radiation.* Academic Press, 392 pp.

Macpherson, B., B. J. Wright, W. H. Hand, and A. J. Maycock, 1996: The impact of MOPS moisture data in the U. K. Meteorological Office mesoscale data assimilation scheme. *Mon. Wea. Rev.,* **124,** 1746–1766.

McMillin, L. M., D. S. Crosby, and M. D. Goldberg, 1995: A water vapor index from satellite measurements. *J. Appl. Meteor.,* **34,** 1551–1558.

McNally, A. P., and M. Vesperini, 1996: Variational analysis of humidity information from TOVS radiances at ECMWF. *Quart. J. Roy. Meteor. Soc.,* **122,** 1521–1544.

Mitchell, H. L., C. Charette, C. Chouinard, and B. Brasnett, 1990: Revised interpolation statistics for the Canadian data assimilation procedure: Their derivation and application. *Mon. Wea. Rev.,* **118,** 1591–1614.

Phalippou, L., 1996: Variational retrieval of humidity profile, wind

speed and cloud liquid-water path with the SSM/I: Potential for numerical weather prediction. *Quart. J. Roy. Meteor. Soc.*, **122B,** 327–355.

Rodgers, C. D., and C. D. Walshaw, 1966: The computation of infrared cooling rate in planetary atmospheres. *Quart. J. Roy. Meteor. Soc.*, **92,** 669–679.

Rothman, L. S., and Coauthors, 1987: The HITRAN database: 1986 edition. *Appl. Opt.*, **26,** 4058–4097.

Salathé, E. P., Jr., D. Chesters, and Y. C. Sud, 1995: Variability of moisture in the upper-troposphere as inferred from TOVS satellite observations and the ECMWF model analyses in 1989. *J. Climate*, **8,** 120–132.

Schmetz, J., and O. M. Turpeinen, 1988: Estimation of the upper tropospheric relative humidity field from Meteosat water vapor image data. *J. Appl. Meteor.*, **27,** 889–899.

——, C. Geijo, W. P. Menzel, K. Strabala, L. van De Berg, K. Holmlund, and S. Tjemkes, 1995: Satellite observations of upper tropospheric relative humidity, clouds and wind field divergence. *Contrib. Atmos. Phys.*, **68,** 345–357.

Soden, B. J., and F. P. Bretherton, 1993: Upper tropospheric relative humidity from GOES-7 channel: Method and climatology for July 1987. *J. Geophys. Res.*, **98**(D9), 16 669–16 688.

——, and ——, 1994: Evaluation of water vapour distribution in general circulation models using satellite observations. *J. Geophys. Res.*, **99**(D1), 1187–1210.

——, and ——, 1996: Interpretation of TOVS water vapor radiances in terms of layer-average relative humidities: Method and climatology for the upper, middle, and lower troposphere. *J. Geophys. Res.*, **101**(D5), 9333–9343.

Stephens, G. L., D. L. Jackson, and I. Wittmeyer, 1996: Global observations of upper-tropospheric water vapor derived from TOVS radiance data. *J. Climate*, **9,** 305–326.

Sullivan, J., L. Gandin, A. Gruber, and W. Baker, 1993: Observation error statistics for *NOAA-10* temperature and height retrievals. *Mon. Wea. Rev.*, **121,** 2578–2587.

Yu, W., L. Garand, and A. P. Dastoor, 1997: Evaluation of model clouds and radiation at 100 km scale using GOES data. *Tellus*, **49A,** 246–262.